RESEARCH ARTICLE

Quantitative Characterization of Respiratory Patterns on Dynamic Higher Temporal Resolution MRI to Stratify Postacute Covid-19 Patients by Cardiopulmonary Symptom Burden

Lea Azour, MD,[1,2*] 🆔 🐦 Henry Rusinek, PhD,[1] Artem Mikheev, BS,[1]

Nicholas Landini, MD, PhD,[3] Mahesh Bharath Keerthivasan, PhD,[4] Christoph Maier, MD, PhD,[1] 🆔

Barun Bagga, MD,[5] Mary Bruno, RT,[1] Rany Condos, MD,[6] William H. Moore, MD,[1] and

Hersh Chandarana, MD[1]

Background: Postacute Covid-19 patients commonly present with respiratory symptoms; however, a noninvasive imaging method for quantitative characterization of respiratory patterns is lacking.

Purpose: To evaluate if quantitative characterization of respiratory pattern on free-breathing higher temporal resolution MRI stratifies patients by cardiopulmonary symptom burden.

Study Type: Prospective analysis of retrospectively acquired data.

Subjects: A total of 37 postacute Covid-19 patients (25 male; median [interquartile range (IQR)] age: 58 [42–64] years; median [IQR] days from acute infection: 335 [186–449]).

Field Strength/Sequence: 0.55 T/two-dimensional coronal true fast imaging with steady-state free precession (trueFISP) at higher temporal resolution.

Assessment: Patients were stratified into three groups based on presence of no ($N = 11$), 1 ($N = 14$), or ≥ 2 ($N = 14$) cardiopulmonary symptoms, assessed using a standardized symptom inventory within 1 month of MRI. An automated lung postprocessing workflow segmented each lung in each trueFISP image (temporal resolution 0.2 seconds) and respiratory curves were generated. Quantitative parameters were derived including tidal lung area, rates of inspiration and expiration, lung area coefficient of variability (CV), and respiratory incoherence (departure from sinusoidal pattern) were. Pulmonary function tests were recorded if within 1 month of MRI. Qualitative assessment of respiratory pattern and lung opacity was performed by three independent readers with 6, 9, and 23 years of experience.

Statistical Tests: Analysis of variance to assess differences in demographic, clinical, and quantitative MRI parameters among groups; univariable analysis and multinomial logistic regression modeling to determine features predictive of patient symptom status; Akaike information criterion to compare the quality of regression models; Cohen and Fleiss kappa (κ) to quantify inter-reader reliability. Two-sided 5% significance level was used.

Results: Tidal area and lung area CV were significantly higher in patients with two or more symptoms than in those with one or no symptoms (area: 15.4 cm² vs. 12.9 cm² vs. 12.8 cm²; CV: 0.072, 0.067, and 0.058). Respiratory incoherence was significantly higher in patients with two or more symptoms than in those with one or no symptoms (0.05 vs. 0.043

vs. 0.033). There were no significant differences in patient age ($P = 0.19$), sex ($P = 0.88$), lung opacity severity ($P = 0.48$), or pulmonary function tests ($P = 0.35–0.97$) among groups. Qualitative reader assessment did not distinguish between groups and showed slight inter-reader agreement ($\kappa = 0.05–0.11$).

Data Conclusion: Quantitative respiratory pattern measures derived from dynamic higher-temporal resolution MRI have potential to stratify patients by symptom burden in a postacute Covid-19 cohort.

Level of Evidence: 3

Technical Efficacy: Stage 3

Dyspnea is a common yet nonspecific respiratory complaint[1] with a variety of cardiopulmonary etiologies.[2,3] Despite its importance, an objective measure correlating with dyspnea is lacking. Dyspnea is one of the most frequent postacute sequelae of Covid-19 infection,[4] with nearly half of postacute Covid-19 patients (those beyond 4 weeks from acute infection[5]) reporting persisting symptoms at 4 months.[6]

Currently, spirometry is considered the reference standard for respiratory functional assessment but it does not provide regional assessment of pulmonary kinetics or evaluate the consistency of the breathing pattern. Functional respiratory impairments on spirometry may also emerge later than morphologic imaging abnormalities, as described with interstitial lung disease,[7] obstructive lung disease,[8] and small airways disease.[9,10]

Quantitative characterization of patients' breathing patterns (including depth, rate, and periodicity) could potentially help diagnose, stratify, and surveil patients. Respiratory pattern can be captured by motion sensors[11,12] or optoelectronic plethysmography[13]; however, similar to spirometry, these techniques do not provide structural lung images. Images using radiography,[14] CT,[15] and MRI[16–18] can be obtained dynamically and have been used to describe diaphragmatic and chest wall motion, a correlate of lung volumes.

Of these modalities, MRI is well-suited for higher temporal resolution dynamic imaging due to lack of radiation and ability to provide morphologic lung data. Until recently, inadequate spatial and temporal resolution, low signal-to-noise ratio, motion artifacts, and signal intensity nonuniformity have precluded automatic lung segmentation and motion processing, particularly during normal breathing.[19] Low field strengths, with increased T1 and T2 signal intensity and decreased susceptibility artifact, may overcome some of these challenges and can also increase patient access due to lower cost and fewer contraindications.[20]

Recent improvements in fast MRI enable dynamic imaging of free-breathing subjects.[21–23] One such method uses a coronal fast imaging with steady-state free precession (trueFISP) chest MR sequence at higher temporal resolution (0.2 seconds). The resulting dynamic data allow for automated processing and quantification of respiratory patterns.[23] Not only has MRI-derived lung volumetry been found to correlate with spirometry,[24–26] but new parameters beyond traditional spirometry-based volumes and rates can be derived from dynamic free-breathing MRI. These parameters have potential to reflect symptomatic disruption of normal breathing patterns and may be clinically relevant.[23]

Thus, the purpose of this study was to evaluate if 1) quantitative characterization of respiratory pattern, and 2) visual assessment by radiologists, on low-field free-breathing dynamic higher temporal resolution MRI stratifies postacute Covid-19 patients by cardiopulmonary symptom burden.
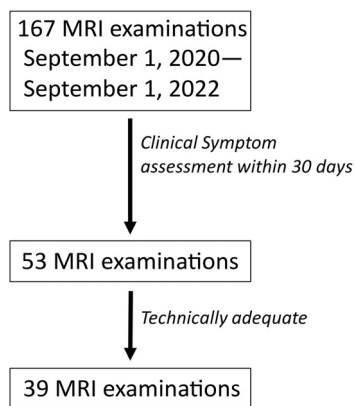
Methods

Patient Selection

This Health Insurance Portability and Accountability Act (HIPAA)-compliant prospective analysis of retrospectively acquired data was approved by the local institutional review board. All patients provided written informed consent.

Postacute Covid-19 patients were recruited for the creation of a multidisciplinary Survivorship Database, which involved the prospective collection of blood, imaging and functional data needed to investigate genetic and immunologic drivers of postacute sequelae of SARS-CoV-2. All patients registered in this database were invited to participate in a research MRI.

For inclusion in this study of respiratory patterns and clinical symptoms, subjects needed to have undergone a dynamic low-field (0.55 T) lung MRI examination within 1 month of a standardized symptom inventory assessment (Figure 1). Of registered participants, 104 were imaged by cardiopulmonary MRI from September 1, 2020 through September 1, 2022 at least once, with a total of 167 examinations acquired. All examinations included a dynamic higher-temporal resolution coronal series for quantitative assessment of respiratory pattern. Of these, 53 MRI examinations were obtained within 1 month of clinical symptom assessment, and 39 examinations were technically acceptable in terms of antero-posterior positioning of the coronal slice at the level of the distal trachea/carina (see MRI Protocol section). Two patients had two examinations; each examination corresponding to a different clinical symptom burden group (described below) at each unique time point.

Demographic and Clinical Assessments

Patient data were collected including sex, age, time from acute Covid-19 infection, and severity of initial infection.

```
┌─────────────────────────┐
│ 167 MRI examinations    │
│ September 1, 2020—       │
│ September 1, 2022        │
└─────────────────────────┘
            │
            │  Clinical Symptom
            │  assessment within 30 days
            ▼
┌─────────────────────────┐
│ 53 MRI examinations     │
└─────────────────────────┘
            │
            │  Technically adequate
            ▼
┌─────────────────────────┐
│ 39 MRI examinations     │
└─────────────────────────┘
```

Figure 1: Flowchart of examinations.

Initial clinical severity of Covid-19 infection was assigned as follows: 1—outpatient; 2—hospitalization not requiring oxygen support; 3—hospitalization requiring oxygen support; and 4—hospitalization requiring mechanical ventilation.

Cardiopulmonary symptoms at follow-up were assessed by a standard symptom inventory questionnaire before or at the clinical visit. Cardiopulmonary symptoms interrogated included chest pain, palpitations, dyspnea at rest, dyspnea on exertion, cough, wheezing, difficulty breathing, fatigue, and lightheadedness. Patients were then stratified into three groups based on the number of reported cardiopulmonary symptoms: group 0: no reported cardiopulmonary symptoms ($N = 11$); group 1: one symptom ($N = 14$); and group 2: two or more symptoms ($N = 14$).

Pulmonary function test (PFT) data within 1 month of MRI were available for 24 corresponding MRI examinations. St. George Respiratory Questionnaire (SGRQ) scores within 3 months of MRI (survey questions refer to a 3-month time frame) were available for 21 MRI examinations.

MRI Protocol

Imaging was performed on a prototype 0.55 T system, modified from a commercial MRI system (MAGNETOM Aera; Siemens Healthcare, Erlangen, Germany). Higher temporal resolution dynamic MR data was acquired using a two-dimensional (2D) trueFISP sequence with a 15-mm thick coronal slice positioned at the level of the distal trachea/carina. Patients were imaged in the supine position during free breathing. They were instructed to breathe comfortably.

Two acquisition protocols were used during the study period, with more recent examinations sacrificing temporal resolution to achieve higher spatial resolution and improve lung parenchymal signal intensity (Figure 2). Twenty examinations were acquired at in-plane resolution 4×4 mm^2, field of view (FOV) 370×450 mm^2, temporal resolution 189.3 msec, flip angle 27°, readout bandwidth 2126 Hz/Px, echo spacing 1 msec, averages 2, and measurement time 51 seconds (protocol 1). Nineteen examinations were

acquired at in-plane resolution 1.8×1.8 mm^2, FOV 450×450 mm^2, temporal resolution 208 msec, flip angle 30°, readout bandwidth 1002 Hz/Px, echo spacing 2.4 msec, and measurement time 77 seconds with 0.1 seconds pause between images. Two hundred and fifty images were acquired in both protocols.

Axial T2-weighted images for opacity characterization were acquired using a prospectively triggered free-breathing turbo spin echo sequence at 5–6 mm slice thickness.

Automated Lung Postprocessing Workflow

A fully automatic lung postprocessing workflow (FireVoxel, www.firevoxel.org) was applied to the anonymized cases, consisting of three steps[22]:

1. Segmenting left and right lung, LL1 and RL1, on the initial time point.
2. Segmenting left and right lung on the entire 250-frame dynamic series.
3. Extracting area-time activity curves for left and right lung.

STEP 1. After signal nonuniformity-correction, locally adaptive thresholding and maximum connected component analysis, a body mask, BM, was extracted from the initial time frame of each dynamic series. A hole-filling operator, followed by extraction of the two largest connected components, then generated the initial left and right lung masks, LL0 and RL0. The lung upper threshold T was calculated as $(S_{\text{Lung}} + S_{\text{Body}})/2$, where S_{Lung} is the average MRI signal within LL0 and RL0 masks and S_{Body} is the average signal in the surrounding chest, defined as the set difference BM − (LLM0 ∪ RLM0). The adjusted lung masks, LL1 and RL1, were then constructed by augmenting the initial lung masks with adjacent voxels with signal intensity below the threshold T (Figure 3a).

STEP 2. Left and right lung regions of interest (ROIs) produced in step 1 were then propagated to the remaining 249 time points using the elastic deformation algorithm. Briefly, elastic deformation is represented as a smooth flow field mapping from frame 1 to frame N. The deformation is computed using dynamic programming applied to the image grid. An image-derived minimum spanning tree was used as a graph structure which allowed efficient computation of the global optimum.[27] Grid sampling was used to evaluate the similarity cost between images. The elastic transformation was modeled using Gaussian radial basis functions. Accuracy of the segmentation was visually confirmed at every time point with mis-segmentation occurring in less than 0.4% of frames.

STEP 3. Once the left and right lung ROIs were constructed for all time points, the area (cm^2) of the lung at each time
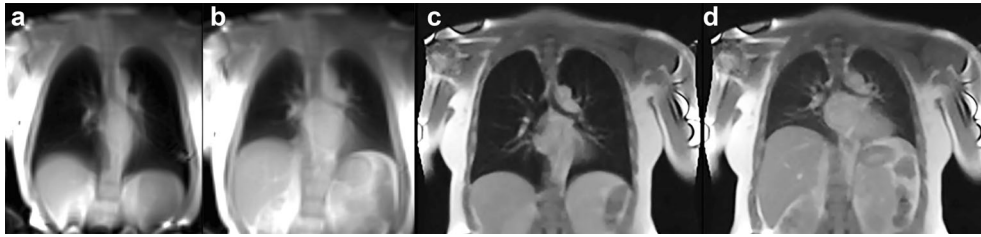
Figure 2: (**a, b**) Protocol 1 dynamic higher temporal resolution coronal MRI image slices acquired during inspiration (left) and expiration (right); in-plane resolution 4×4 mm^2 and temporal resolution 189 msec. (**c, d**) Protocol 2 dynamic higher temporal resolution coronal MRI image slices acquired during inspiration (left) and expiration (right); in-plane resolution 1.8×1.8 mm^2 and temporal resolution 208 msec.
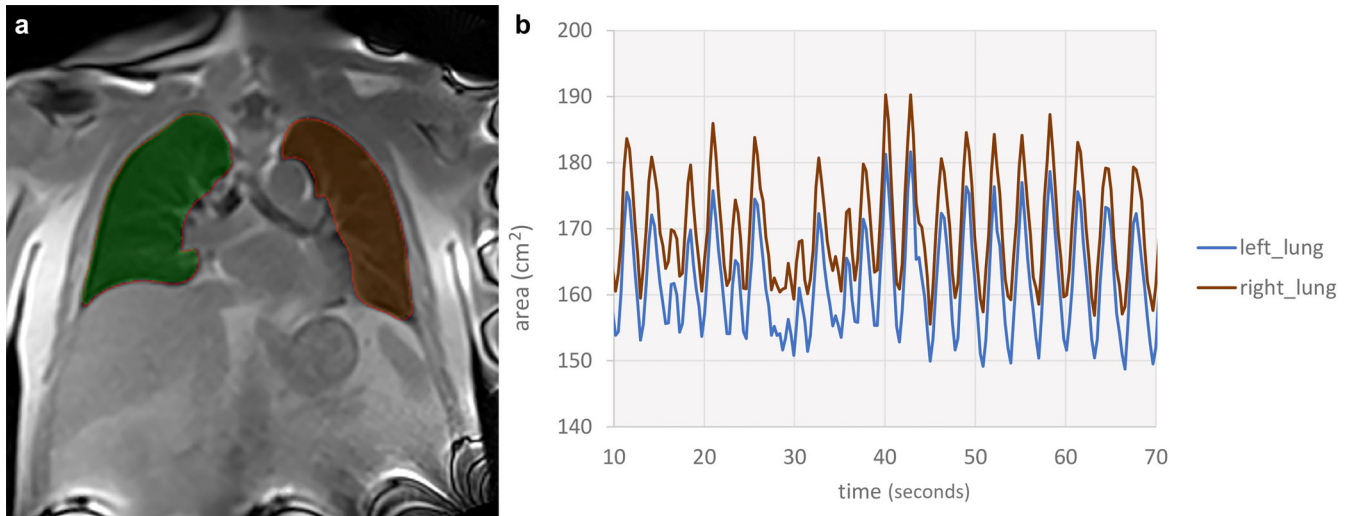

Figure 3: (**a**) Coronal image demonstrating automated green and orange segmentation overlays of the right and left lungs, respectively. (**b**) Respiratory curves derived from the dynamic MRI acquisition for each lung in a single subject (y-axis lung area in cm^2; x-axis time in seconds).

point was calculated, yielding the time area curves. These time area, or respiratory, curves (Figure 3b) were used to calculate lung parameters.

Derivation of Quantitative Parameters for Characterization of Respiratory Pattern

Quantitative parameters were derived for each lung. Several parameters have been explored in a pilot study as promising markers of dyspnea.[23] Based on these early results, we evaluated five respiratory measures: tidal lung area, average rate of inspiration, average rate of expiration, lung area coefficient of variability (CV), and respiratory incoherence.

Inspiration and expiration slopes were computed as the rate of change of lung area (i.e., increase for inspirations and decrease for expirations) in cm^2/second, averaged over all breaths. These values were normalized to the mean lung area.

CV of lung area during breathing cycles was also normalized to the mean lung area. An area CV of 0.05 corresponded to a standard deviation of 5% from the mean.

Breathing can be characterized in terms of respiratory rate, depth, and constancy, which together comprise a pattern. Respiratory incoherence is a parameter that captures the

regularity (or irregularity) of the breathing pattern, which is independent of patient size.[23] It is a measure of the departure of the respiratory curve from periodicity, or expected rhythmic pattern of normal breathing. The nominal period p is selected from all possible values of p that leads to minimal root mean square error. A periodic curve, of any period and any shape, will have an incoherence value of zero. Lower values indicate better respiratory regularity, and higher values signify greater departure from respiratory regularity.

Assessment of Potential Bias Due to Protocol Change

Because two imaging protocols were used in this prospective analysis of retrospectively acquired data, we assessed the effect of image resolution on computed parameters by downsampling examinations from 1.8 mm (protocol 2) to 4 mm (protocol 1) in-plane resolution, followed by re-interpolating temporal sampling. This procedure was applied to nine randomly selected dynamic datasets acquired with protocol 2, with three examinations selected from each of the three clinical groups. For each selected examination and each of the 250 time points, image data were resampled to simulate a

corresponding examination that would be acquired using protocol 1. We then measured the effect of protocol change on the respiratory measures. Spatial downsampling was implemented to incorporate the partial volume effect. Spline interpolation was used to simulate the change in temporal resolution from 208 to 190 msec.

Qualitative Reader Assessment

Three readers of varying experience level (WHM 23 years, BB 9 years, and CM 6 years) subjectively assessed lung opacity, variability in respiratory rate, variability in respiratory amplitude, and size of amplitude, independently and blinded to patient information.

MRI lung opacity was scored on axial T2-weighted image series (Visage PACS; Visage Imaging, San Diego, CA, USA). Scoring was based on percent opacification by lung quadrant on a scale of 0–4, yielding summed total opacity scores ranging 0–16 for each examination. This low-field MRI opacity scoring system has been previously described and has shown moderate and fair inter-reader, and moderate to substantial inter-modality concordance with CT, for characterizing the presence and extent of groundglass opacities.[28] A quadrant score of 1 represented less than 25% opacity, a score of 2 represented 25 to <50% opacity, a score of 3 represented 50 to <75% opacity, and a score of 4 corresponded to ≥75% opacity in the quadrant.

Variability in breathing frequency was graded on a scale of 1–4, as follows: 1: no variability, a consistent breathing rate; 2: minor variability, one or two episodes of rate change described as either faster or slower breathing episodes; 3: moderate variability, three to five episodes of rate change; and 4: severe variability with no consistent breathing rate or five or more episodes of rate change.

Variability in breathing amplitude was graded on a scale of 1–4, as follows: 1: no variability, consistent breathing amplitude; 2: minor variability, one or two episodes of amplitude change described as 25% or greater change in amplitude; 3: moderate variability, three to five episodes of amplitude change; 4: severe variability, no consistent breathing amplitude or five or more episodes of amplitude change.

Respiratory amplitude (craniocaudal excursion) was graded on a scale of 1–5, as follows: 1: moderate to severely reduced amplitude; 2: mildly reduced amplitude; 3: normal amplitude; 4: mildly increased amplitude; and 5: moderate to severely increased amplitude.

Statistical Analysis

Analysis of variance (ANOVA) and Turkey's honestly significance difference test was used to assess differences in demographic, clinical, quantitative, and qualitative imaging-based respiratory parameters among the three patient groups stratified by symptom burden. The F-value was derived to assess variation in samples. Univariable analysis and multinomial logistic regression modeling were used to determine features predictive of patient symptom burden as expressed by clinical grouping 0 (no symptoms), 1 (1 symptom), and 2 (≥2 symptoms). Two predictive models were generated, a model based on clinical parameters (age, sex, and BMI) and a model based on the MRI quantitative parameters. The Akaike information criterion (AIC) was used to compare the quality of regression models based on cohort data. Intraclass correlation coefficient and root mean square error were computed to assess the effect of MRI acquisition protocol change on respiratory metrics. Inter-reader reliability was calculated using Cohen and Fleiss kappa (κ), with ≤0 = no agreement; 0–0.2 = slight agreement; 0.2–0.4 = fair agreement; 0.4–0.6 = moderate agreement; 0.6–0.8 = substantial agreement; and 0.8–1 = almost perfect agreement.[29] All statistical tests were conducted at the two-sided 5% significance level using R version 4.2.2 software.

Results

Thirty-nine MRI examinations were acquired in 37 individuals (25 men, 12 women; median age 58, interquartile range [IQR] 42–64; Table 1) with history of Covid-19 pneumonia, and symptom inventory within 1 month (median 21 days, IQR 11.5–25.5 days). All MRI examinations were acquired in the postacute Covid-19 setting at median 335 days (IQR 186–449 days) from acute infection.

MRI examinations were stratified into three groups based on patients' reported cardiopulmonary symptoms: group 0: no reported cardiopulmonary symptoms ($N = 11$); group 1: one symptom ($N = 14$); and group 2: two or more symptoms ($N = 14$; Table 2). There were no significant differences in patient age ($P = 0.19$) or sex ($P = 0.88$) among the three groups stratified by symptom burden (Table 2).

The most frequently reported symptoms were dyspnea on exertion (18/39, 46.2%) and fatigue (15/39, 38.5%). There were no significant differences among the three clinical groups in terms of imaging protocol ($P = 0.783$) or total lung opacity severity score ($P = 0.484$; Figure 4), see Table 2.

SGRQ symptom scores ($N = 21$; group 0 = 5, group 1 = 8, and group 2 = 8) were significantly higher in group 2 than group 0 ($P = 0.044$, 95% confidence interval 0.7–61.8; Table S1), with a trend of increasing scores between the three ordinally ordered groups.

PFTs ($N = 24$; group 0 = 7, group 1 = 9, group 2 = 8) did not significantly differ between the groups (Table S1): percent total lung capacity p = 0.969; percent functional residual capacity p = 0.598; percent residual volume p = 0.346; percent forced vital capacity (FVC) p = 0.394; percent forced expiratory volume in 1 second (FEV$_1$) p = 0.521; FEV1/FVC p = 0.574; diffusing capacity of carbon monoxide (DLCO) p = 0.603; and percent DLCO p = 0.886.

Table 1. Cohort Characteristics	
	$N = 37$ individuals[a]
Age (years), median (IQR)	58 (42–64)
Sex, N (%)	
M	25 (68)
F	12 (32)
Race, N (%)	
Asian	4 (11)
Black or African American	3 (8)
Native Hawaiian or Pacific Islander	1 (3)
White	26 (70)
Other	1 (3)
Unknown/Not reported	2 (5)
Ethnicity, N (%)	
Hispanic/Latino	4 (11)
Not Hispanic or Latino	27 (73)
Unknown/Not reported	6 (16)
Initial clinical severity, N (%)	
Outpatient	19 (51)
Hospitalized, without oxygen requirement	1 (3)
Hospitalized, with nonmechanical ventilation oxygen requirement	11 (30)
Hospitalized, with mechanical ventilation	6 (16)
Disease course, N (%); number of days (IQR)	
History of hospitalization	28 (49); 9.5 [5–23]
History of ICU admission	9 (23); 12 [5–36]
History of mechanical ventilation	6 (16); 20 [6–28]
MRI examinations, $N = 39$, number of days (IQR)	
Interval from initial Covid-19 illness to MRI	335 (186–449)
Interval between MRI and Symptom Inventory	21 (11.5–25.5)*

Values in N (%), unless otherwise specified.
*Absolute days, before or after.
[a]The two patients with two examinations were in different symptom groups at each unique time point.

Quantitative MRI Respiratory Pattern Features by Symptom Burden

Several quantitative MRI-based respiratory measures differentiated between patient groups stratified by symptom burden (Table 3, Figure 5). Group averages changed in a monotonic fashion between groups 0, 1, and 2 for tidal area, area CV, and incoherence.

Tidal area differentiated between patient groups stratified by symptom burden. Group 2 had significantly higher tidal area than Group 1 and Group 0 (15.4 cm^2 vs. 12.9 cm^2 vs. 12.8 cm^2). Area CV differentiated between patient groups; individuals with more symptoms had significantly higher variability in lung area than those with one or no symptoms (0.072 vs. 0.067 vs. 0.058).

Respiratory incoherence differentiated between patient groups stratified by symptom burden. Group 2 had significantly higher respiratory incoherence than patients with one or no symptoms (0.0495 vs. 0.0426 vs. 0.0334). There was no significant difference between inspiratory ($P = 0.363$) and expiratory slope ($P = 0.842$) between symptom burden groups.

A multivariable multinomial logistic model to predict symptom burden (groups 0, 1, 2) based on the five quantitative respiratory features (Table 3) had 74.4% accuracy, and AIC 30.8. The accuracy of a model based on demographic and clinical predictors (age, sex, BMI) was 46%, with AIC of 38.1.

Impact of Protocol on Quantitative Features

Table 4 demonstrates good agreement between respiratory features computed from protocol 1 and data acquired with protocol 2 downsampled to simulate the spatial and temporal resolution of protocol 1. Intra-class correlations coefficients were all higher than 0.93. The percent root mean square error for the two most sensitive features, respiratory area CV and incoherence, were both less than 2.5%, which is small compared to >10% mean values changes across clinical groups (Table 3).

Qualitative Reader Assessment of Respiratory Variability

For each of the 3 readers, there was no significant association between qualitative assessment of variability in respiratory rate, variability in respiratory amplitude, or size of respiratory amplitude among symptom groups (Table S2).

There was significant but slight inter-reader agreement for qualitative ratings of variability in breathing rate ($\kappa = 0.11$) and variability in breathing amplitude ($\kappa = 0.11$). The inter-reader agreement for size of respiratory amplitude was not significant ($\kappa = 0.05$, $P = 0.33$; Table 5).

Table 2. Groups Stratified by Protocol, Symptoms, and Total Opacity Score

	Group 0 ($N = 11$)	Group 1 ($N = 14$)	Group 2 ($N = 14$)	$P*$
Age	49.5 ± 14.3	59.4 ± 10.4	53.7 ± 15.1	0.19
Female sex, N (%)	8 (73)	9 (64)	10 (71)	0.88
Protocol				
1: 190 msec, 4×4 mm^2	6	8	6	0.783
2: 206 msec, 1.8×1.8 mm^2	5	6	8	
Cardiopulmonary symptoms				
Dyspnea at rest	0	2 (14)	6 (43)	0.026*
Dyspnea on exertion	0	5 (36)	13 (93)	<0.0001*
Chest pain	0	1 (7)	6 (43)	0.011*
Palpitations	0	0 (0)	4 (29)	0.028*
Cough	0	1 (7)	7 (50)	0.004*
Wheeze	0	0 (0)	0 (0)	NA
Difficulty breathing		0 (0)	1 (7)	NA
Fatigue	0	5 (36)	10 (71)	0.001*
Lightheadedness	0	0 (0)	2 (14)	0.320
Total opacity score[a]				
Reader 1	6.55 ± 5.11	5.71 ± 4.32	5.43 ± 4.01	0.817
Reader 2	9.09 ± 5.19	6.07 ± 4.65	9.29 ± 5.69	0.209
Reader 3	5.82 ± 2.96	4.86 ± 2.21	5.36 ± 3.37	0.710
Average all readers	7.15 ± 3.62	5.55 ± 3.37	6.69 ± 3.43	0.484

Values in N (%), unless otherwise specified.
*$P < 0.05$. P-value corresponds to the Fisher's exact test for independence of categorical variables. Unlike for chi-square test, these P-values are reliable even if the expected count of participants with symptoms is small. Groups are defined as 0: no symptoms; 1: 1 symptom; 2: ≥2 symptoms.
[a]Mean + SD. The total opacity score was treated as a numeric variable and group means were compared using one-way analysis of variance.

Discussion

In this study, the ability of quantitative respiratory pattern features derived from dynamic higher-temporal resolution MRI to stratify patients by symptom burden was investigated in a postacute Covid-19 cohort. Lung area CV and respiratory incoherence monotonically increased with symptom burden. However, qualitative assessment of variability in respiratory rate and amplitude lacked sufficient inter-reader reliability and did not distinguish between symptom groups, supporting the need for automated quantitative pipelines.

Unlike measurements from spirometry, the MRI metrics of incoherence and lung area CV are not influenced by body size or respiratory effort. Further, they quantify respiratory pattern variability, which is not currently assessed by spirometry or other routine diagnostic testing.

As in previous studies, contemporaneous lung opacity severity did not correlate with the presence or severity of patient symptoms,[30] or lung function.[31] However, we found that dynamic parameters did correlate with patient-reported symptom. In a cohort of 33 post-Covid patients of whom 45% reported dyspnea, a previous study reported that while PFTs were not significantly different, dynamic electrical impedance tomography showed higher regional ventilatory inhomogeneity in the symptomatic patients.[32] Dynamic MRI in 27 post-Covid patients has also shown differences in ventilation compared to a group of 12 healthy volunteers, and Covid-19 survivors showed regional high ventilation areas and breathed more deeply during supine tidal breathing at rest than normal volunteers.[33] In the current study, tidal area also increased with increasing symptom burden. Symptomatic
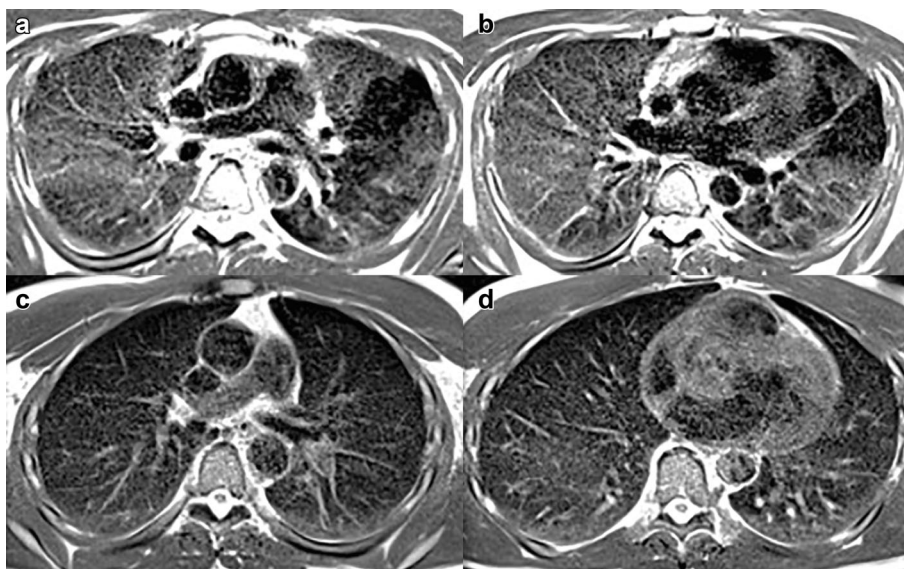
Figure 4: (a, b) Asymptomatic patient. T2-weighted axial images through the lungs show diffuse bilateral lung opacities and total opacity score of 12; only portions of the lingula and anteromedial basilar left lower lobe are spared. The patient had a respiratory incoherence measure of 0.0202; values closer to 0 indicate more regular breathing. (c, d) Severely symptomatic patient. T2-weighted axial images through the lungs show no appreciable pulmonary opacity (total opacity score of 2 likely representing dependent atelectasis). The patient had a relatively high respiratory incoherence value of 0.0474, signifying a departure from a regular breathing pattern.

Table 3. Quantitative MRI Respiratory Pattern Features for Stratification by Symptom Burden

Feature	Group 0 Avg ± SD	Group 1 Avg ± SD	Group 2 Avg ± SD	P ANOVA	Group 2– Group 0 95% Confidence Interval	P Group 2 vs 0
Tidal area (cm^2)	12.8 ± 2.6	12.9 ± 2.9	15.4 ± 3.5	0.0287*	0.011, 5.89	0.0489*
Inspiratory slope	0.093 ± 0.024	0.106 ± 0.020	0.106 ± 0.030	0.363	−0.012, 0.037	0.427
Expiratory slope	−0.073 ± 0.023	−0.078 ± 0.019	−0.079 ± 0.029	0.842	−0.029, 0.018	0.844
Area CV	0.0583 ± 0.0093	0.0670 ± 0.0122	0.0724 ± 0.0155	0.0341*	0.0014, 0.0267	0.0264*
Incoherence	0.0334 ± 0.0064	0.0426 ± 0.0110	0.0495 ± 0.0185	0.0188*	0.0029, 0.0293	0.0138*

*$P < 0.05$.

patients in our cohort may have demonstrated larger tidal areas due to feelings of breathlessness or air hunger, which are associated with altered breathing patterns.[34]

Patient position may influence diaphragmatic motion and lung volumes which may be reflected in measures of tidal area. Diaphragmatic movement has been found to be higher, and lung volumes lower, in the supine position.[35,36] This may mean patient position can influence the performance of MRI quantitative respiratory features. Quantitative parameters that are not based on absolute differences (like length, area, volume, or rate), but instead reflect variability or pattern deviation (like CV or incoherence) may prove more robust and independent of patient position.

While tidal area may relate to the PFT parameter tidal volume, tidal area does not characterize the *pattern* of breathing, which was assessed in the current study by the features lung area CV and incoherence. Our findings showed higher area CV and higher incoherence in symptomatic patients, indicating the greater irregularity of their breathing pattern.

Altered breathing patterns instigating intermittent or chronic respiratory or nonrespiratory symptoms[34] have been termed "dysfunctional breathing." Incoherence in
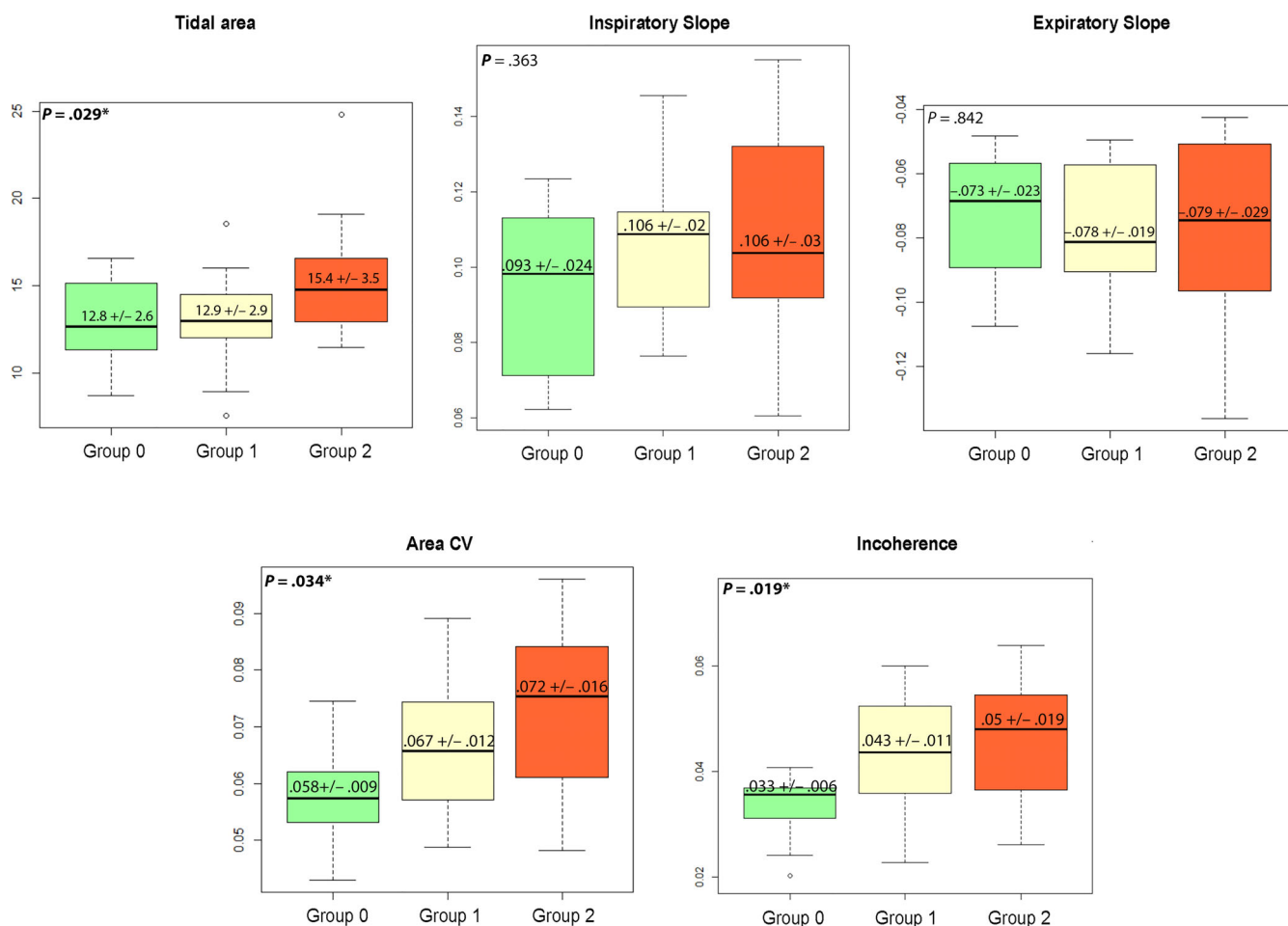
Figure 5: Distribution of quantitative MRI respiratory pattern features among patients stratified by symptom burden. Box plots demonstrating monotonic increases in median values between group 0, group 1, and group 2 for tidal area, area CV, and incoherence, signifying progressively larger tidal area, variability in tidal area, and variability in respiratory pattern in patients with higher symptom burden. Numeric values correspond to group means and standard deviation. *P-value, ANOVA.

Table 4. Effect of Protocol Change

Quantitative Feature	ICC	95% Confidence Interval	P	RMSE%
Tidal area	0.937	(0.745, 0.986)	<0.0001	9.8%
Inspiratory Slope	0.959	(0.830, 0.990)	<0.0001	7.7%
Expiratory Slope	0.933	(0.680, 0.985)	0.00016	7.9%
Area CV	0.994	(0.974, 0.999)	<0.001	2.4%
Incoherence	0.999	(0.995, 1.000)	<0.001	2.5%

ICC: intraclass correlation coefficient; RMSE: root mean square error, considering higher-resolution protocol 2 results as true values.

symptomatic patients may reflect quantification of previously described features of dysfunctional breathing, like deep sighs,[34] or other manifestations of dyspnea like rapid breathing. Dyspneic patients with obstructive disease more often endorse respiratory distress, while those with restrictive disease describe rapid breathing.[37]

Using structured light plethysmography, Sakkatos et al demonstrated the relevance of quantifying breathing pattern, showing that within-subject variability of respiratory timing metrics correlated with asthma control in a cohort of 122 subjects.[38] Patients with uncontrolled asthma showed higher breathing variability.[38] Functional data analysis of breathing

Table 5. Inter-Reader Reliability

Qualitative Feature	All Readers		R1 and R2		R2 and R3		R1 and R3	
	κ	P	κ	P	κ	P	κ	P
Variability in respiratory rate	0.111	0.0438	0.152	0.0838	0.202	0.0126	0.019	0.846
Variability in respiratory amplitude (craniocaudal excursion)	0.109	0.0477	0.295	0.000585	0.070	0.42	0.004	0.969
Size of respiratory amplitude	0.051	0.33	0.126	0.0324	0.096	0.0701	0.094	0.352

patterns via opto-electronic plethysmography has also been used to classify patients based on respiratory pathophysiology.[13]

MRI may enable assessment of breathing pattern quantitatively, noninvasively, and without radiation, while also providing regional lung morphology. Additional regional metrics quantifying ventilation/perfusion[31,33,39] or deformation[40] may also be derived by MRI. Low-field technology increases patient accessibility, being lower-cost in terms of magnet siting and maintenance, lower specific absorption rate, and technical parameters favorable to lung imaging.[20]

Limitations

First, this study was conducted in a small cohort of postacute Covid-19 patients. Despite the small sample size, statistically significant differences were found in quantitative metrics characterizing respiratory pattern. Second, two different imaging protocols were used to acquire data in this study. However, using downsampling and spline interpolation to simulate a cohort with both protocols, there were minimal changes in MRI quantitative features. The impact of temporal gaps, the 0.1 seconds pause between images in protocol 2, on curve analysis are a limitation that can be addressed in future investigation. Third, in this study, we used a faster 2D single slice technique, rather than examining lung volumes from a three-dimensional or multi-slice acquisition; the use of a volumetric technique and/or more posterior coronal slice positioning to include a larger lung volume requires future investigation. Further developments may also include regional lung analysis, assessment of instructed deep breathing maneuvers, and the effect of patient position. Last, because our findings are currently specific to this Covid-19 cohort, similar investigations in patients with other respiratory diseases are necessary to determine generalizability of this method.

Conclusion

Quantitative respiratory pattern measures derived from dynamic higher-temporal resolution MRI have potential to stratify patients by symptom burden in a postacute Covid-19 cohort. This study demonstrates the potential for quantitative MRI to provide an anatomic and physiologic/functional explanation for patient respiratory symptoms.

Acknowledgments

Data Availability Statement

Data generated or analyzed during the study are available from the authors by request.

References

1. Parshall MB, Schwartzstein RM, Adams L, et al. An official American Thoracic Society statement: Update on the mechanisms, assessment, and management of dyspnea. Am J Respir Crit Care Med 2012;185: 435-452.

2. Ryan JJ, Waxman AB. The dyspnea clinic. Circulation 2018;137:1994-1996.

3. Huang W, Resch S, Oliveira RKF, Cockrill BA, Systrom DM, Waxman AB. Invasive cardiopulmonary exercise testing in the evaluation of unexplained dyspnea: Insights from a multidisciplinary dyspnea center. Eur J Prev Cardiol 2017;24:1190-1199.

4. Chen C, Haupert SR, Zimmermann L, Shi X, Fritsche LG, Mukherjee B. Global prevalence of post-coronavirus disease 2019 (COVID-19) condition or long COVID: A meta-analysis and systematic review. J Infect Dis 2022;226:1593-1607.

5. Chippa V, Aleem A, Anjum F. Post-acute coronavirus (COVID-19) syndrome. StatPearls. 2023.

6. O'Mahoney LL, Routen A, Gillies C, et al. The prevalence and long-term health effects of long Covid among hospitalised and non-hospitalised populations: A systematic review and meta-analysis. EClinicalMedicine 2023;55:101762.

7. Showalter K, Hoffmann A, Rouleau G, et al. Performance of forced vital capacity and lung diffusion cutpoints for associated radiographic interstitial lung disease in systemic sclerosis. J Rheumatol 2018;45:1572-1576.

8. Regan EA, Lynch DA, Curran-Everett D, et al. Clinical and radiologic disease in smokers with normal spirometry. JAMA Intern Med 2015; 175:1539-1549.

9. Hogg JC. Pathophysiology of airflow limitation in chronic obstructive pulmonary disease. Lancet 2004;364:709-721.

10. Hoesterey D, Das N, Janssens W, et al. Spirometric indices of early airflow impairment in individuals at risk of developing COPD: Spirometry beyond FEV1/FVC. Respir Med 2019;156:58-68.

11. Solomon E, Rigie DS, Vahle T, et al. Free-breathing radial imaging using a pilot-tone radiofrequency transmitter for detection of respiratory motion. Magn Reson Med 2021;85:2672-2685.

12. Vahle T, Bacher M, Rigie D, et al. Respiratory motion detection and correction for MR using the pilot tone: Applications for MR and simultaneous PET/MR examinations. Invest Radiol 2020;55:153-159.

13. LoMauro A, Colli A, Colombo L, Aliverti A. Breathing patterns recognition: A functional data analysis approach. Comput Methods Programs Biomed 2022;217:106670.

14. Yamada Y, Ueyama M, Abe T, et al. Time-resolved quantitative analysis of the diaphragms during tidal breathing in a standing position using dynamic chest radiography with a flat panel detector system ("dynamic X-ray phrenicography"). Acad Radiol 2017;24:393-400.

15. Brennan D, Schubert L, Diot Q, et al. Clinical validation of 4DCT-ventilation with pulmonary function test data. Int J Radiat Oncol Biol Phys 2015;92:423-429.

16. Gierada DS, Curtin JJ, Erickson SJ, Prost RW, Strandt JA, Goodman LR. Diaphragmatic motion: Fast gradient-recalled-echo MR imaging in healthy subjects. Radiology 1995;194:879-884.

17. Von Siebenthal M, Székely G, Gamper U, Boesiger P, Lomax A, Cattin P. 4D MR imaging of respiratory organ motion and its variability. Phys Med Biol 2007;52:1547-1564.

18. Von Siebenthal M, Gattin P, Camper U, Lomax A, Székely G. 4D MR imaging using internal respiratory gating. Med Image Comput Comput Assist Interv 2005;8(Pt 2):336-343.

19. Tokuda J, Schmitt M, Sun Y, et al. Lung motion and volume measurement by dynamic 3D MRI using a 128-channel receiver coil. Acad Radiol 2009;16:22-27.

20. Campbell-Washburn AE, Ramasawmy R, Restivo MC, et al. Opportunities in interventional and diagnostic imaging by using high-performance low-field-strength MRI. Radiology 2019;293:384-393.

21. Bhave S, Lingala SG, Newell JD, Nagle SK, Jacob M. Blind compressed sensing enables 3D dynamic free breathing MR imaging of lung volumes and diaphragm motion. Invest Radiol 2016;51:387-399.

22. Mikheev A, Wake N, Rusinek H, Chandarana H. Single-lung dynamics assessed using XD-GRASP MRI and automatic segmentation. In: *Proceedings of the International Society for Magnetic Resonance in Medicine, 27th Annual Meeting & Exhibition*. Montreal. 2019.

23. Azour L, Mikheev A, Rusinek H, et al. Dysfunctional respiratory patterns in symptomatic post-acute Covid-19 patients on dynamic high temporal resolution free-breathing lung MRI. In: *Proceedings of the International Society for Magnetic Resonance in Medicine 31st Annual Meeting and Exhibition*. Toronto, Canada. 2023.

24. Plathow C, Schoebinger M, Fink C, et al. Evaluation of lung volumetry using dynamic three-dimensional magnetic resonance imaging. Invest Radiol 2005;40:173-179.

25. Plathow C, Ley S, Fink C, et al. Evaluation of chest motion and volumetry during the breathing cycle by dynamic MRI in healthy subjects: Comparison with pulmonary function tests. Invest Radiol 2004;39: 202-209.

26. Swift AJ, Woodhouse N, Fichele S, et al. Rapid lung volumetry using ultrafast dynamic magnetic resonance imaging during forced vital capacity maneuver: Correlation with spirometry. Invest Radiol 2007;42: 37-41.

27. Heinrich MP, Jenkinson M, Brady M, Schnabel JA. MRF-based deformable registration and ventilation estimation of lung CT. IEEE Trans Med Imaging 2013;32:1239-1248.

28. Azour L, Condos R, Keerthivasan MB, et al. Low-field 0.55 T MRI for assessment of pulmonary groundglass and fibrosis-like opacities: Inter-reader and inter-modality concordance. Eur J Radiol 2022;156:110515.

29. McHugh ML. Interrater reliability: The kappa statistic. Biochem Med 2012;22:276-282.

30. Chang MC, Lee W, Hur J, Park D. Chest computed tomography findings in asymptomatic patients with COVID-19. Respiration 2020;99: 748-754.

31. Lévy S, Heiss R, Grimm R, et al. Free-breathing low-field MRI of the lungs detects functional alterations associated with persistent symptoms after COVID-19 infection. Invest Radiol 2022;57:742-751.

32. Scaramuzzo G, Ronzoni L, Campo G, et al. Long-term dyspnea, regional ventilation distribution and peripheral lung function in COVID-19 survivors: A 1 year follow up study. BMC Pulm Med 2022;22:408.

33. Wang C, Li H, Xiao S, et al. Abnormal dynamic ventilation function of COVID-19 survivors detected by pulmonary free-breathing proton MRI. Eur Radiol 2022;32:5297-5307.

34. Boulding R, Stacey R, Niven R, Fowler SJ. Dysfunctional breathing: A review of the literature and proposal for classification. Eur Respir Rev 2016;25:287-294.

35. Katz S, Arish N, Rokach A, Zaltzman Y, Marcus EL. The effect of body position on pulmonary function: A systematic review. BMC Pulm Med 2018;18:1-16.

36. Takazakura R, Takahashi M, Nitta N, Murata K. Diaphragmatic motion in the sitting and supine positions: Healthy subject study using a vertically open magnetic resonance system. J Magn Reson Imaging 2004; 19:605-609.

37. Elliott MW, Adams L, Cockcroft A, Macrae KD, Murphy K, Guz A. The language of breathlessness. Use of verbal descriptors by patients with cardiopulmonary disease. Am Rev Respir Dis 1991;144:826-832.

38. Sakkatos P, Bruton A, Barney A. Changes in quantifiable breathing pattern components predict asthma control: An observational cross-sectional study. Asthma Res Pract 2021;7:5.

39. Heiss R, Tan L, Schmidt S, et al. Pulmonary dysfunction after pediatric COVID-19. Radiology 2023;306:e221250.

40. Chassagnon G, Martin C, Marini R, et al. Use of elastic registration in pulmonary MRI for the assessment of pulmonary fibrosis in patients with systemic sclerosis. Radiology 2019;291:487-492.